The ST22 chronology for the Skytrain Ice Rise ice core - part 1: A stratigraphic chronology of the last 2000 years

Helene M. Hoffmann[1], Mackenzie M. Grieman[1], Amy C.F. King[2], Jenna A. Epifanio[4], Kaden Martin[4], Diana Vladimirova[2], Helena Pryer[1], Emily Doyle[1], Axel Schmidt[3], Jack D. Humby[2], Isobel F. Rowell[1], Christoph Nehrbass-Ahles[1], Elizabeth R. Thomas[2], Robert Mulvaney[2], and Eric W. Wolff[1]

[1]Dept. of Earth Sciences, University of Cambridge, Downing St, Cambridge CB2 3EQ
[2]British Antarctic Survey, High Cross, Madingley Rd, Cambridge CB3 0ET
[3]Federal Institute of Hydrology, Am Mainzer Tor 1, 56068 Koblenz
[4]College of Earth, Ocean, and Atmospheric Sciences, Oregon State University, Corvallis, OR, USA.

Correspondence: Helene M. Hoffmann (hmh52@cam.ac.uk)

Abstract. A new ice core was drilled in West Antarctica on Skytrain Ice Rise in field season 2018 / 2019. This 651 m ice core is one of the main targets of the WACSWAIN (WArm Climate Stability of the West Antarctic ice sheet in the last INterglacial) project. A present-day accumulation rate of 13.5 cm w.e./year was derived. Although the project mainly aims to investigate the last interglacial (115-130 ka BP), a robust chronology period covering the recent past is needed to constrain the age models for the deepest ice. Additionally, this time period is important for understanding current climatic changes in the West Antarctic region. Here, we present a stratigraphic chronology for the top 184.14 m of the Skytrain ice core covering the last 2000 years based on absolute age tie points interpolated using annual layer counting encompassing the last 2000 years of climate history. Together with a model-based depth-age relationship of the deeper part of the ice core, this will form the ST22 chronology. The chemical composition, dust content, liquid conductivity, water isotope concentration and methane content of the whole core was analysed via continuous flow analysis (CFA) at the British Antarctic Survey. Annual layer counting was performed by manual counting of seasonal variations in mainly the sodium and calcium records. This counted chronology was informed and anchored by absolute age tie points, namely, the tritium peak (1965 CE) and six volcanic eruptions. Methane concentration variations were used to further constrain the counting error. A minimal error of $\pm$ 1 year at the tie points was derived, accumulating to $\pm$ 5-10% of the age in the unconstrained sections between tie points. This level of accuracy enables data interpretation on at least decadal timescales and provides a solid base for the dating of deeper ice, which is the second part of the chronology.

1 Introduction

Detailed investigations of past climate, especially developments in the last 2000 years, provide an important benchmark, capturing both natural and anthropogenic climate change. Ice cores, especially from polar regions, are some of the most powerful environmental archives for palaeoclimate studies for several reasons. One of these reasons is that they record many climatic parameters simultaneously, including small air samples of past atmospheres trapped in tiny air bubbles (e.g. MacFarling Meure et al. (2006); Mitchell et al. (2013)). Linking instrumental climate observations (e.g. Bromwich et al. (2013), Dalaiden et al.

(2020)) with ice core data reaching further back in time is a powerful tool for assessing the processes that contribute to ongoing climatic change. As with any other environmental archive, this use of ice cores as climate archives requires the development of reliable and precise chronologies and depth-age relationships with well-constrained uncertainties.

25   For polar ice cores, there are three main dating approaches, which are combined when possible to establish a robust chronology: (1) the identification and counting of recurring annual stratigraphic features (chemical and physical) in the ice core (Rasmussen et al., 2006; Sigl et al., 2016; Winstrup et al., 2019); (2) flow modeling based on the physical parameters of the glacier on which the ice core was drilled (e.g. (Parrenin et al., 2004)); and (3) the identification of absolute time markers, which is used either to anchor or support these relative dating methods. The most common age markers are sulfate peaks (Castellano et al., 2005; Sigl et al., 2015) or tephra layers (Dunbar et al., 2003; Tetzner et al., 2021; Emanuelsson et al., 2022) caused by

30   volcanic eruptions, but radiometric markers or cosmogenic events like the bomb peak in 1965 CE (Morishima et al., 1985), solar storms (Mekhaldi et al., 2015) or the Laschamps event (Loulergue et al., 2007) can also be used. Their imprint, for example, in the tritium or ^{10}Be content of the ice, can be utilised to tie the annual-layer-counted and ice flow-modeled chronologies to a particular absolute date. These markers are also useful to assess the uncertainties of the layer counting.

35   The ice core investigated in this study was drilled as part of the WArm Climate Stability of the West Antarctic ice sheet in the last INterglacial (WACSWAIN) project. This project aims to decipher the, so far unclear, fate of the West Antarctic Ice Sheet (WAIS) and the Filchner-Ronne Ice Shelf (FRIS) during the Last Interglacial (LIG), which was the last natural warm period, $\sim$ 120 000 years before present. For this purpose, an ice core was drilled at Skytrain Ice Rise (Fig. 1), a location that is adjacent to both WAIS and FRIS, but that, according to modelling studies (DeConto and Pollard, 2016), likely remained

40   ice-covered during the LIG. Here we present the first part of a chronology for the Skytrain ice core. We focus on the last 2000 years contained in the top 200 m and use a combined approach of annual layer counting and the identification of absolute age markers, namely the tritium peak and volcanic eruptions. High resolution methane data is used to further support and verify the chronology. This depth-age relationship for the last 2000 years will be used to constrain a chronology of the deeper part of the core, which is discussed in our companion paper (Mulvaney et al., 2022) currently in preparation.

45 **2   Methods**

2.1   The WACSWAIN ice core

The drilling site (79°44.46′ S, 78°32.69′ W) for the ice core at Skytrain ice rise in West Antarctica was selected based on initial ground penetrating radar exploration that showed a well-pronounced Raymond arch and undisturbed layering within the study area (Mulvaney et al., 2021). The mean annual surface air temperature at the site is -26°C, so no substantial influence

50   of surface melt was expected. The surface elevation at the drilling site is 784 m above sea level (a.s.l.). The core was drilled to bedrock during the 2018/19 field season and has a total length of 651 m. Each 80-cm core piece was weighed to calculate density. The depth of bubble close-off, determined by high resolution discrete total air content analysis, was reached at 58 m total core depth. Dielectric profiling (DEP) measurements (Wilhelms et al., 1998) were carried out on each core piece before processing.
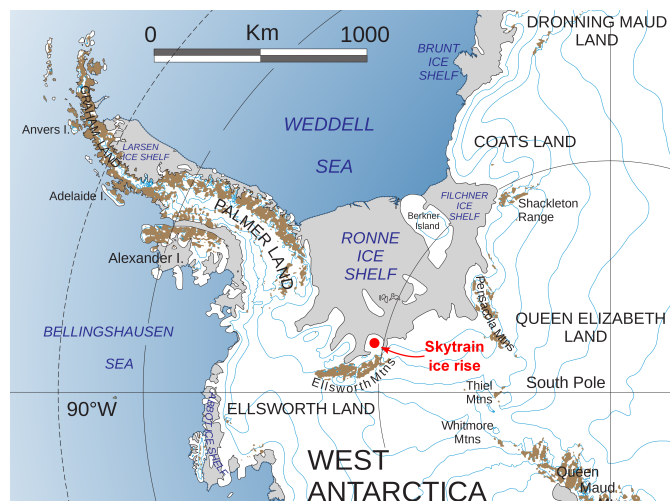
Figure 1. Map of West Antarctica and the Ronne Ice Shelf (modified from USGS (1999)) showing the drilling site (arrow) of the ice core drilled on Skytrain Ice Rise.

2.2 Continuous Flow Analysis

Chemical analyses of the Skytrain ice core were carried out at the British Antarctic Survey (BAS) in Cambridge via continuous flow analysis (CFA). This setup comprises an inductively-coupled plasma mass spectrometer (ICP-MS) for ^{23}Na, ^{24}Mg, ^{27}Al, ^{43}Ca, ^{44}Ca, two fast ion chromatography (FIC) systems for anion and cation analysis, a particle counter, a fluorescence detection setup for H_2O_2, NH_4^+ and Ca^{2+}, two conductivity meters and two Picarro spectrometers; one for online stable water isotope analysis and one for methane concentration analysis (Grieman et al., 2021). An overview of the instruments and their specifications is given in Table 1.

A schematic of the entire CFA setup is given in Fig. 2. Longitudinal CFA sticks of 3.2 cm x 3.2 cm x 80 cm were cut from the whole length of the ice core using a band saw in a cold room. The ends of each stick and every break surface were scraped before melting to reduce contamination. The sticks were continuously melted at a speed of about 3.5-4 cm/min in the firn section, $\sim$ 3 cm/min for the middle section of the core, and $\sim$ 1.6 cm/min for the basal 100 m. The electrically-heated melthead consists of 5 melt water lines, 4 outer and one inner, of which only the central one was used for analysis (see also Fig. 2). The whole length of the core was analysed. Calibration of the ICP-MS, FICs, fluorescence and water isotope instrument was performed at the beginning and the end of each measurement day using standard solutions of known chemical and isotopic composition. Further information on limits of detection, sensitivity and the standardisation process can be found in (Grieman et al., 2021).

Both FIC systems for cation and anion analysis were run parallel, sampling from the same core depth interval. Both FICs consist of two internal measurement systems. They use a dual column system. Each of the two 1.0 mL sample loops was loaded sequentially from the continuous meltwater stream at a flow rate slightly above 1.0 mL min^{-1}. For the anion detection,

Table 1. Overview of the instrument specifications used in the continuous flow analysis of Skytrain ice core. The values given for depth resolution of the ICP-MS, FIC and fluorescence instruments were determined in (Grieman et al., 2021). The other values were estimated during the Skytrain CFA measurement campaign. The term Depth resolution refers to the minimal depth interval (layer thickness) that can be resolved by the respective method. The column Points per mm refers to the number of data points recorded per millimeter of ice core at an average melt speed for the respective instrument throughout the last 2000 years.

Instrument	Model	Analytes	Depth resolution	Points per mm
ICP-MS	Agilent 7700x	^{23}Na, ^{24}Mg, ^{27}Al, ^{43}Ca, ^{44}Ca	3.8-4.7 cm	2.9
FIC cation	Dionex ICS-3000	Na$^+$, Ca^{2+}, Mg^{2+}, NH$_4^+$, K$^+$	> 4cm	-
FIC anion	Dionex ICS-6000	NO$_3^-$, F$^-$, MSA, Cl$^-$, SO$_4^{2-}$	> 4cm	-
Fluorescence	FIALab Precision Measurement Technologies photomultiplier tube fluorometers (PMT-FL)	Ca^{2+}, NH$_4^+$, H$_2$O$_2$	1.4 cm	1.7
Particle counter	Abakus (Klotz)	Dust content (particles)	< 2 cm	1.7
Conductivity	Amber Science, Inc. 3082 series	liquid conductivity	< 2 cm	1.7
Conductivity	Dionex conductivity detector (CDM-1)	liquid conductivity	< 2 cm	1.7
Water isotopes	Picarro L2130-i CRDS	^{18}O, D	5-10 cm	1.6
Methane	Picarro G2301 CRDS	CH$_4$	> 10 cm	1.6

Figure 2. Schematic of the CFA setup at the BAS ice core analysis lab. The meltwater from the inner part of the core is distributed to 12 different analytical systems. The small numbers on the lines denote meltwater flow rates in mL/min.

a Dionex ICS-6000 fast ion chromatography (FIC) system with conductivity detection was used. The sample was separated using Dionex AS15 (5 μm, 3 x 150 mm) columns and a 60 mM NaOH eluent. A similar approach for anion detection was used in the field before (Schüpbach et al., 2018). Details on the cation system can be found in Grieman et al. (2021). The depth resolution of the ICP-MS analysis is a running average of about 4 cm for Na, Mg and Ca. The depth resolution of the fluorescence calcium detection was found to be $\sim$ 1.4 cm. The FIC instruments have a theoretical depth resolution of about 4 cm, but one sample was measured every 2.63 cm (Grieman et al., 2021) and not continuously. At this resolution, an annual layer thickness of at least 5 cm was estimated to be distinguishable using the ICP-MS method. The fluorescence calcium detection method was estimated to be able to detect layers with a minimum thickness of 2 cm. These depths resolutions, meaning the capability of the respective system to resolve layers down to a certain thickness, are mainly dominated by smoothing effects in the tubing and the interfaces and not by the measurement capabilities of the instruments themselves (see Table 1, column Points per mm). The depth assignment of each dataset was calculated by combining the melt speed, measured by vertical dislocation of the encoder on top of the melting stick, the flow rates and the measured time delays from the melt head to the respective instruments. The top and bottom depth measured for each core piece during the cutting of the core were used, so there are no propagating depth errors with increasing core depth. The time at which each break in the ice core reached the melthead was manually recorded in Labview by the system operator. Time delays for each instrument were then added to these recorded times to determine instrument analysis times for each ice core break depth. The melt rate was used to adjust ice core depths assigned to instrument analysis times between each break. If this melt rate correction resulted in depth assignments deeper than the depth of the following break or if the meltrate was not recorded, then an evenly-spaced depth scale was applied between ice core breaks.

To determine time delays between the melthead and the instruments, the liquid conductivity data on a depth scale estimated using no time delay was compared to DEP data at the same depths for each CFA measurement day; because DEP was measured directly on the solid core, its depth is assumed to be correct. First the depth scale of the liquid conductivity was assigned using the variable meltspeed readout from the decoder as described above. Any unexpected spikes in this recorded meltrate were removed by interpolation. The MATLAB "xcorr" function was then used to estimate a depth "lag" between the two datasets for each CFA day. This depth lag is an estimate of the time delay between the melthead and the conductivity detectors. The depth assignments of the liquid conductivity, dust, and fluorescence Ca^{2+} measurements were corrected using this depth lag. The ICP-MS calcium data on an instrument analysis time scale for each CFA measurement day were then compared to the raw fluorescence Ca^{2+} data. The "xcorr" function was used to estimate the analysis time delay between the fluorescence Ca^{2+} measurements and the ICP-MS calcium measurements. The sum of this time delay and the time delay calculated for the depth shift of the calcium fluorescence data was used to shift the instrument analysis time of the ICP-MS and cation and anion FIC raw data before applying the depth scale to the raw data.

(a)   (b)
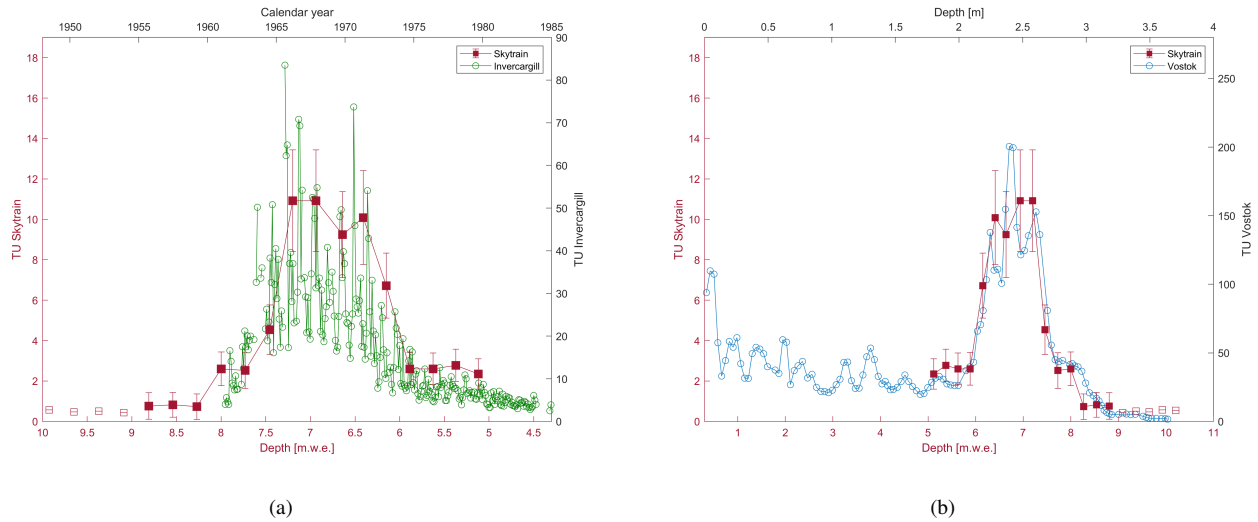
Figure 3. Tritium analysis of the Skytrain ice core (red squares) compared to (a) Invercargill precipitation concentration (green circles) and (b) snowpit data from Vostok station (Antarctica) (blue circles) (Fourré et al., 2018). The samples denoted by open squares were below the detection limit (< 0.7 TU).

2.3 Absolute age markers

2.3.1 Tritium analysis

Every chronology of an environmental archive that was established using relative stratigraphic counting techniques requires absolute age markers to verify the counted age over depth and to evaluate the corresponding age uncertainty. Vast amounts of anthropogenic tritium (^{3}H) were injected into the atmosphere by thermonuclear explosions from the late 1950s until the partial test ban treaty became effective in 1963 CE., with some tests continuing after that. This tritium emission has been reported to be globally-distributed and was found in Antarctic snow samples (Taylor, 1964), where it still could be detected 15 years ago. (Fourré et al., 2006). 20 firn samples between 10.4 and 18.95 m depth were selected for tritium analysis. This depth range was chosen based on a first estimation of the accumulation rate from seasonal variations in the water isotope signal of snowpit samples from the drilling site and the initial annual layer counting using the sodium ICP-MS signal. The ^{3}H content of the meltwater was measured at the Federal Institute of Hydrology in Koblenz, Germany (sample data in Table A1). The samples were distilled, and tritium was electrolytically enriched. The tritium concentration was measured by low background liquid scintillation counting (Quantulus GCT 6220) with a detection limit of about 0.7 TU (Schmidt et al., 2020) .

Tritium concentrations were found to be very low (< 12 TU), but measurable. The results are shown in Fig. 3, along with tritium concentrations that were measured in precipitation at Invercargill (NZ) and in a snowpit at Vostok station (Antarctica) in 2008 (Fourré et al., 2018). The peak of the Skytrain tritium concentration (10.92 TU) was visually matched with the peak concentrations in the precipitation data. Based on this visual comparison, the year 1965 CE was identified at a depth of 7.2 m

w.e. in the Skytrain ice core. As an important result, the near-surface accumulation rate could be derived to be 13.5 cm w.e / year.

2.3.2 Volcanic eruptions

125 One of the most commonly used age markers in ice cores are the chemical and physical signatures of well-dated, global or hemispheric volcanic eruptions (Sigl et al., 2015). These eruptions can be identified as peaks in acidity from the DEP signal or in the non sea salt sulfate concentration (Castellano et al., 2005). On the East Antarctic plateau these volcanic signatures are very distinct and are visible as clear peaks above the background sulfate concentration. (Baroni et al., 2008). However, the geographic location in West Antarctica and the comparably low elevation of the Skytrain ice core mean that this site is much
130 more influenced by marine air masses with large inputs of marine biogenic and sea salt sulfate (e.g. Dixon et al. (2004)). This difference is also confirmed at two near-by ice cores from the Antarctic Peninsula, where high background biogenic sulfate overwhelms the volcanic signal (Emanuelsson et al., 2022). As such, the Skytrain ice core shows high and variable sulphate levels, and it is not possible to definitively identify volcanic eruptions from the DEP or CFA data. This issue has also been reported for other near-coastal ice core sites and can restrict the use of volcanic tie-points in stratigraphic age models (Philippe
135 et al., 2016; Winstrup et al., 2019).

Therefore, this study used a new method to identify volcanic eruptions from the sulfur (S) isotope composition of sulfate (from now on denoted SO_4^{2-}) in the ice. Volcanic S emissions have been shown to have distinctive, isotopically-light values compared to other dominant inputs from sea-salt or marine biogenic SO_4^{2-}(Rees et al., 1978; Nielsen et al., 1991; Patris et al., 2000), meaning that S isotope analyses can be used to determine which SO_4^{2-} peaks have a volcanic origin and define
140 the precise depth of volcanic tie-points. Sulfur (S) isotope analyses were conducted at the Department of Earth Sciences at the University of Cambridge Isotope Group clean laboratories using a Thermo Scientific Neptune Plus™multi-collector inductively coupled mass spectrometer (MC-ICP-Ms) Potential depth intervals were selected from the depth of the tritium peak, the initial layer counting, and the identification of peaks in $SO_4^{2-}$from the CFA data. The ice was cut into 5-7 cm length sections and scraped with a razor blade to remove potential surface contaminants. An aliquot of these samples was measured for discrete
145 SO_4^{2-}concentrations on the IC, and then the volume needed to target 30 nmol of $SO_4^{2-}$was transferred to acid-clean Teflon vials and evaporated to dryness at 80°C. The samples were resuspended in 70 μl of ultra-pure water (resistivity > 18 MΩ cm) and passed through anion-exchange columns following methods adapted from Burke et al. (2019) to separate the $SO_4^{2-}$from other components in the ice.

All measurements on the MC-ICP-MS were made in high-resolution mode, using an Aridus introduction system. We used
150 standard-sample bracketing protocols with Na_2SO_4 to account for mass-bias and instrumental drift following the method developed by Paris et al. (2013). S isotope compositions were reported using $\delta^x S$ notation, as the difference of either the $^{34}S/^{32}S$ or $^{33}S/^{32}S$ ratio of each sample from the Vienna-Canyon Diablo Troilite (VCDT) in parts per mille (‰) (Equation 1).

$$\delta^x S = \frac{(\delta^x S/\delta^{32} S)_{sample}}{(\delta^x S/\delta^{32} S)_{standard}} - 1 \qquad (1)$$

The relative deviation between the δ^{33}S and δ^{34}S ratios was calculated using Δ^{33}S notation (Equation 2), where values outside analytical error of zero indicate mass-independent fractionation (Farquhar et al., 2001). Mass-independent fractionation of S occurs when sulfur dioxide is photo-oxidised to SO_4^{2-} by short-wave UV radiation above the ozone layer (Savarino et al., 2003), meaning that non-zero Δ^{33}S values can be used as a marker of stratospheric volcanic eruptions (Gautier et al., 2019), (Burke et al., 2019).

$$\Delta^{33}S = \delta^{33}S - ((\delta^{34}S + 1)^{0.515} - 1) \tag{2}$$

All samples were measured at least in triplicate. Long-term reproducibility was quantified by repeated measurements of an H_2SO_4 ICP-MS standard (δ^{34}S = +3.13 ‰, σ = 0.06, n = 26) and IAPSO seawater (δ^{34}S = +21.18 ‰, σ = 0.09, n = 26), which showed good agreement to published values from multiple previous studies (Craddock et al., 2008; Das et al., 2012). Conservative errors of $\pm$ 0.20 ‰ and $\pm$ 0.15 ‰ were assigned to all δ^{34}S and Δ^{33}S values, respectively, equalling $\pm$ 2 σ variability of repeat measurements of standards and replicate samples.

These analyses allowed for a clear distinction between background and volcanic S isotope compositions and the identification of the exact depth interval of well-dated volcanic eruptions. The samples interpreted to reflect background conditions had δ^{34}S values ranging from + 15.86 to + 18.76 ‰ (mean = + 17.43 ‰), and the samples defined as volcanic had values ranging from - 12.31 to + 14.32 ‰ (mean = +5.64 ‰). Many of the volcanic samples also showed mass-independent fractionation (range Δ^{33}S = - 1.36 to + 0.93 ‰), whereas all background Δ^{33}S values were within analytical error of zero, giving additional evidence to define the depth of stratospheric volcanic eruptions.

A total of 43 samples were analysed and seven volcanic events were identified (Table B1), corresponding to the 1815 CE eruption of Tambora, the 1458 CE eruption of Kuwae, and four eruptions at 1285 CE, 1276 CE, 1257 CE and 1229 CE from the Samalas sequence (Sigl et al., 2015). A peak potentially representing an eruption of unknown origin in 1110 CE was also identified. Examples of the peak selection for volcanic tie-points are shown in Figure 4.

2.3.3 Methane measurements

To further constrain the layer counted chronology below the depth of the deepest confidently-identified volcanic eruption (1229 CE, 97.45 m), we measured methane concentrations in the Skytrain ice core and compared them to the high resolution WAIS Divide ice core methane dataset (Mitchell et al., 2011; Koehler et al., 2017). In total, 39 discrete Skytrain ice core samples from the archive piece (quarter core) were selected at 1.5-1.6 m depth intervals between 84 m and 143.20 m, working around any cracks and breaks to achieve the best ice quality for gas analysis. This depth interval overlaps with the presumed depth of the 1257 CE volcanic eruption sequence.

The samples were analysed at Oregon State University (USA) using a melt and refreeze wet-extraction technique as described in detail in Grachev et al. (2009), Mitchell et al. (2011), and Lee et al. (2020). In brief, samples of approximately 10 x 3 x 3 cm (long side orientated vertically along the core) were sealed in individual glass vacuum flasks and attached to the extraction line. The extraction procedure is automated to give exact replication of the method for each sample. The samples are firstly kept frozen in an ethanol bath while evacuating the flasks to vacuum. A warm water bath then melts the samples,
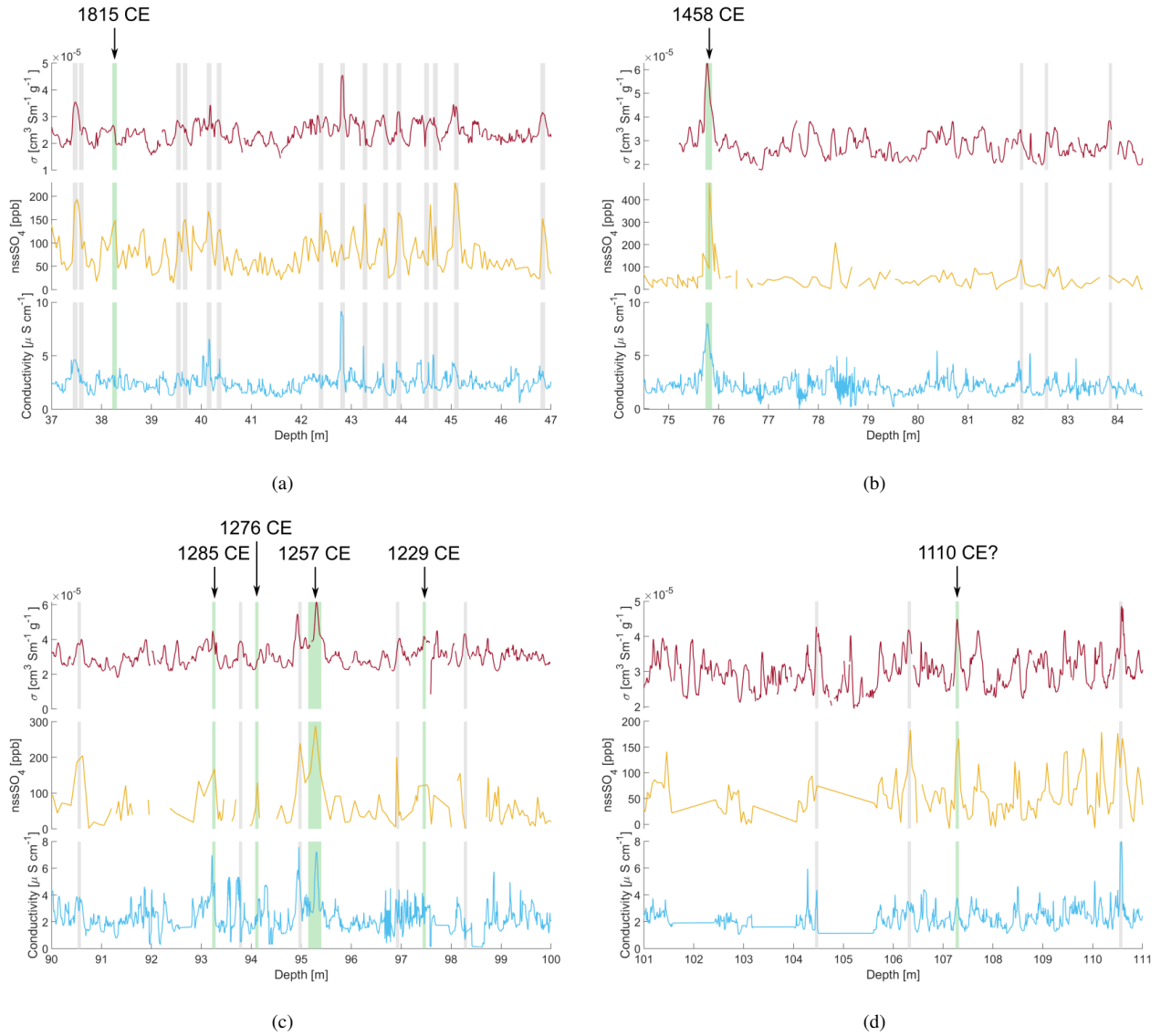
Figure 4. Examples of the depth selection for δ^{34}S sampling for identification of volcanic eruptions based on DEP (density corrected, top), FIC sulfate (middle) and CFA liquid conductivity (bottom) signals. (a) shows the peak selected for identification of the 1815 CE Tambora eruption,(b) for 1458 CE, (c) shows the peaks selected for identification of the 1257 CE eruption sequence of four (1229, 1257, 1276 and 1285 CE) and (d) for a potential 1110 CE eruption. The green bars denote the samples that could be identified as volcanic. The grey bars denote other samples that were analysed in the search for the respective eruption.

releasing the trapped air into the headspace above the melt water. Refreezing of the samples, again in an ethanol bath, precedes expansion of the extracted air into a gas chromatograph (GC) for measurement of the CH_4 concentration. Expansion is repeated four times per sample. All concentrations were referenced to the WMO X2004A reference scale (Dlugokencky et al., 2005) and

190   were calibrated using a NOAA primary air standard with a calibrated concentration of 481.25 ppb CH_4. Final concentrations were corrected by subtraction of an average background value of 8.25 ppb, determined by expanding the air standard over gas-free ice samples that are measured using the same procedure as described above. A solubility correction accounts for the small portion of air that remains dissolved in the melt water and is therefore not extracted, following the derivation in (Mitchell et al., 2013). 1 ppb was added to each sample to account for the solubility, giving the final CH_4 value.

195   Two true-depth replicate samples are usually measured in this method. However, available ice resulted in only one sample of large enough volume for the required methodology. As a result, one measurement per depth level is presented here. Given the strong validation of the method in previous studies, the requirement for only matching overall CH_4 trends as opposed to absolute values of CH_4 for this dating purpose, and the good correspondence of the trends observed in the Skytrain CH_4 in comparison to the WAIS record, this is determined to be satisfactory. The overall uncertainty of the CH_4 data presented here is

200   estimated to be 2-3 ppb, based on errors of previous studies using the same analytical system where duplicate measurements were available (Mitchell et al., 2011, 2013; Epifanio et al., 2020).

    Additionally, methane concentrations were analyzed continuously in a 17 m-long ice core section (144-161 m) adjoining the discrete sample section on the deeper end using the BAS CFA system and a Picarro G2301 CRDS instrument. Similar to the CH_4 dissolution effect described for the discrete CH_4 data, the continuously measured data is always lower than the actual

205   atmospheric value because a small amount of air dissolves in the melt water on its way to a hydrophobic membrane module (Fig. 2). Absolute values of this highly resolved continuous data are typically assigned using a few discretely measured CH_4 'anchor' points. Unfortunately, we do not have any discrete CH_4 data for the depth section that was measured in a continuous fashion. However, we calibrated the instrument's output by measuring NOAA primary air standards (405.8 ppb and 869.1 ppb CH_4 calibrated against WMO X2004A reference scale (Dlugokencky et al., 2005)) and checked for linearity ($R^2 = 0.998$)

210   using a working gas standard (602.0 ppb). We then made daily calibrations mimicking gas extraction from melt water through a full loop using degassed de-ionised water and the working gas standard. Therefore, CH_4 values were calibrated to the NOAA scale using a slope of 0.970 and an intercept of -6.278. We estimated the dissolution factor to increase the raw measurements by 8.73%. The instrumental CFA CH_4 uncertainty is 10 ppb.

    The combined discrete and continuous methane concentrations from 84 to 161 m were then matched to the high resolution

215   CH_4 data from the WAIS Divide ice core (Fig. 5). The variations of the WAIS CH_4 record on the gas age scale were visually aligned with the Skytrain CH_4 on its depth scale. Seven tie points were manually identified (Table C1) and are shown by the dashed lines in Figure 5. Subsequently the WAIS Divide ice core gas age (WD2014, (Sigl et al., 2019)) was assigned to the corresponding Skytrain ice core depth. To determine the gas-age ice-age difference (delta age), the age difference between the derived Skytrain ice core gas ages and the matching volcanic tie point ice ages in the depth interval between 84 and 98 m were

220   calculated . This delta age was found to be about 300 years. The delta age was then added to all the matched gas ages to convert them into the respective ice ages. Please note that it is beyond the scope of this paper to establish and analyse the full gas age
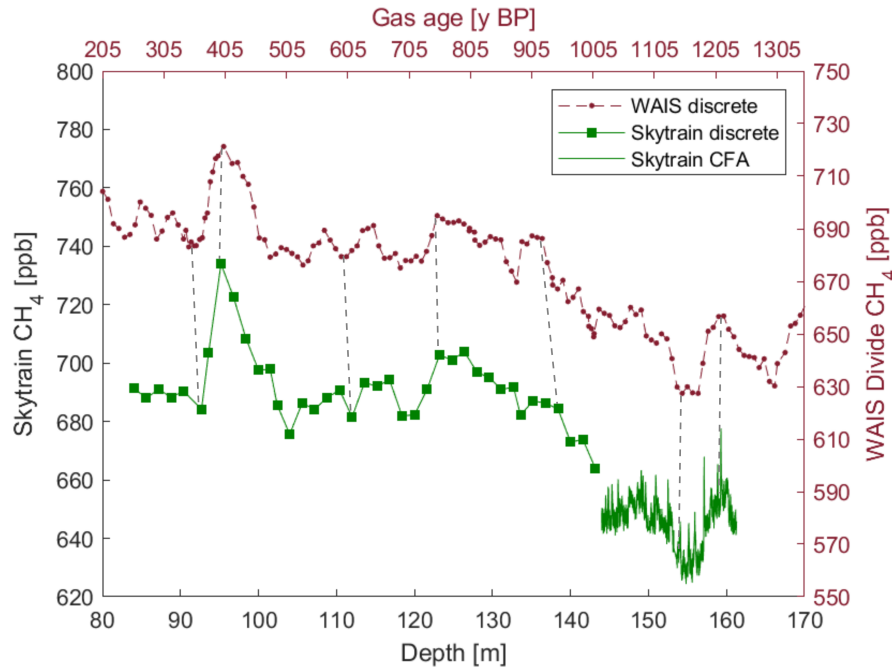
Figure 5. Skytrain methane measurements compared to WAIS Divide ice core methane measurements (Mitchell et al., 2011). The green squares denote discrete Skytrain methane measurements completed at OSU. The green line shows the continuous methane concentrations analyzed using the BAS CFA system. The Skytrain ice core methane record on a depth scale was compared visually to best fit the variability of the WAIS record on its age scale (WD2014) (Sigl et al., 2019). The selected tie points are marked by the grey dashed lines connecting the shown records.

chronology of Skytrain ice core. Here the methane data was used to support the annual layer counted ice age chronology. The full gas age scale based on CFA methane measurements will be addressed in the companion paper.

3 Core chronology

3.1 Layer identification

3.1.1 Manual identification

It should be noted that the layer identification in the Skytrain Ice Core was generally challenging, mainly because of the high noise and (marine) background levels of the respective species. This is a feature of the site and not caused by the analytical methods. We therefore would like to emphasize that the annual layer counting only serves as an interpolation between the absolute age markers and does not stand as a chronology alone. Annual layers were identified using chemical species that are known to show seasonal variations in concentration. Because of the comparably high and variable (mainly marine) background
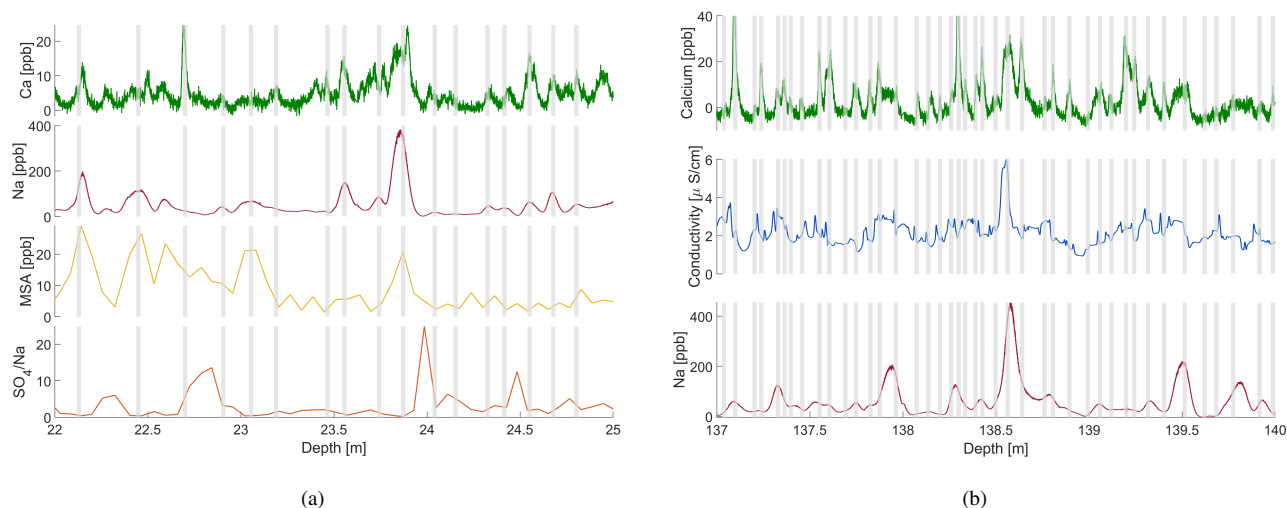
Figure 6. Skytrain ice core chemical records from (a) 15-18 m ($\sim$ 1952 - 1961 CE) and (b) 140-143 m ($\sim$ 713-752 CE). Above $\sim$ 70 m, annual layers were identified by common peaks in Na (ICP-MS signal) and MSA (FIC signal) along with minima in SO_4^{2-} (FIC)/Na ratios. Below $\sim$ 70 m, calcium concentrations were used as the primary annual layer indicator. The grey bars denote the identified annual layers.

of many chemical species (e.g. sulfate) in the Skytrain ice core, it was not sensible to apply automated layer identification algorithms like StratiCounter (Winstrup et al., 2012). Instead, the counting was performed manually using Matchmaker, a graphical MATLAB application, which allows annual layer counting of multiple records simultaneously (Rasmussen et al.,

235 2008). Some of the most common parameters used to investigate seasonal variations and to identify annual layers in the firn section of Antarctic ice cores are the H_2O_2 concentration and stable water isotope ratios (Schlosser and Oerter, 2002; Sigg and Neftel, 1988). However, in the Skytrain ice core, these parameters only show a seasonal cycle in the top 10-15 m of the core. Below 15 m, both signals become too smoothed to resolve annual variability. Sodium and MSA (methanesulfonic acid) also commonly show seasonal variability in Antarctic ice cores. Sodium concentrations peak in the austral winter layer,

240 due to the combined influence of sea ice emissions and increased transport, and MSA peaks in the austral summer due to enhanced biological activity (e.g. (Sigl et al., 2016; Osman et al., 2017)). In the Skytrain ice core, MSA peaks at the same time as sodium. This phenomenon of migration into winter snow layers has been observed before (Pasteur and Mulvaney, 2000). Conversely, sulfate concentrations are highest in the austral summer (Preunkert et al., 2008). Therefore, minima in the SO_4^{2-}/Na ratio coincide with maxima in sodium and MSA and are used in this study to underpin the identification of annual

245 layers. An example of Na (ICP-MS), MSA (FIC) and SO_4^{2-} (FIC)/Na data along with calcium concentrations from fluorescence detection at the same depths are shown in Figure 6. Another parameter which is known to show seasonal variations in coastal antarctic sites is nitrate (Wagenbach et al., 1988). However, this parameter was also measured using the FIC system and did not have an advantage in terms of depth resolution compared to the MSA. Measured intensities were low and therefore this component was not considered as an annual marker.

250 The proposed relationship between the markers described above is clearly visible in the data. In particular, parallel annual variations in MSA and Na concentrations are distinct. This variability strongly suggests that the measured sodium signal is showing seasonal variability. Sodium was therefore used as the primary indicator for annual layer counting of the top $\sim$ 60-70 m. Below $\sim$ 60-70 m, annual layers in the MSA and SO_4^{2-}/Na signals could no longer be identified due to the limited depth resolution of the FIC method. The sodium-derived depth-age relationship also became linear below $\sim$ 70 m

255 and no longer followed the exponential shape expected due to thinning. This linearity is due to the limited depth resolution of the ICP-MS measurements. However, Figure 6 (a) shows that there is a strong correlation between the higher resolution fluorescence calcium signal and the sodium signal, which has also been observed in other Antarctic ice core records (e.g. (Curran et al., 1998)). Based on this finding, below $\sim$ 60-70 m, calcium was used as the primary indicator for seasonal variations, in combination with sodium and liquid conductivity (Fig. 6 (b)). It was aimed to achieve a gradual transition

260 between the primary markers by attempting to slowly include more peaks from the calcium signal into the sodium count until the calcium record became the primary seasonal indicator. Therefore an exact depth for the shift cannot be given. Below a depth of $\sim$ 200 m, the depth-age relationship of the calcium signal also became linear, which suggests that the limit of the fluorescence calcium depth resolution (1.4 cm) was reached. Further counting would only have resulted in an increasing and hard to determine age uncertainty.

265 **3.1.2 Power Spectra**

To support our findings of the manual layer identification, similar to the approach in Bigler et al. (2011) we calculated simple power spectra for the most important components (Na, Ca, MSA and conductivity) in two different depth intervals (Fig. 7).

In the shallow part, the sodium and MSA power spectra show clear maxima around 10-15 cm layer thickness, which is in good agreement with the findings from the manual layer identification. Also the calcium data shows enhanced values around

270 10-15 cm, but less distinct. The two large peaks in the MSA data between 2-3 cm must be attributed to noise in the measurement and can not refer to actual layers. In the deeper part of the core, the maxima in the power spectra are less obvious, mainly due to the expected higher noise level. There is a clear, rather wide maximum in the Ca record between about 4-12 cm layer thickness, which corresponds well to the layer thicknesses that have been identified manually in this depth section (see also Fig. 8). Also in the conductivity record there is a small maximum around 5 cm layer thickness, matching the findings from the manual layer

275 counting. Remarkably, all records of Na, Ca and liquid conductivity show rather pronounced maxima between about 40-45 cm layer thickness. These variations might hint to some decadal variations. An in depth discussion of these features is however beyond the scope of this study.

3.2 Strategy for integration of absolute age markers and layer counting

The absolute age markers, including the date of the tritium peak, the volcanic eruptions, and the methane measurements, were

280 regarded as intermediate reference points in the layer counting procedure. While the depth of the tritium peak and the positions of the volcanic eruptions were considered to be robust with a small age error (< 1 year), the methane reference points are less well-defined, mainly because of the uncertainties in the assumed delta age of the gas record. Above 13.5 m, the depth of
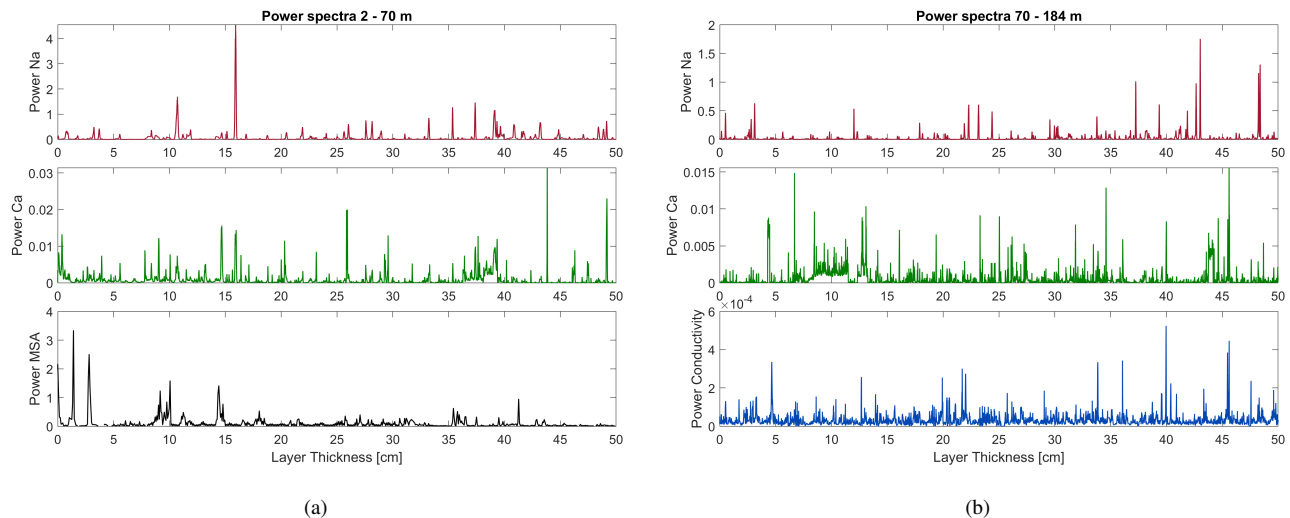
Figure 7. Power spectra for Na, Ca, MSA and conductivity for two different depth intervals. (a) shows the shallow part of the core (0-70 m) and (b) the deeper part (70-184 m). In the shallow part, clear peaks in the sodium and the MSA data around 10 and 15 cm are visible. In the deep part, some variations around 40-45cm layer thickness are dominant, but also a distinct maximum in the CA-data between 4-12 cm layer thickness is visible.

the 1965 CE tritium peak was used as a fixed starting point to calibrate the layer identification procedure. In the first test, the counting was performed using the Na, MSA and SO_4^{2-}/Na ratios as described above. The deviation from 1965 CE in the initial
285   counting attempt was roughly 10%. In a second counting run, the layer counting was adjusted to fit the position of the 1965 CE peak to 1 year. The same strategy was subsequently applied to fit the dates of volcanic eruptions. For this deeper part below 13.5 m, initial calibration of the layer count was performed between the well-defined depths of the 1285 CE, 1257 CE and 1229 CE volcanic eruptions. Peak identification in this section mainly relied on the calcium fluorescence and the conductivity signals. After these two initial tunings of the counting procedure, layer counting below 13.5 m was continued back in time
290   to meet the 1815 CE Tambora eruption depth and consecutively further to 1458 CE. As explained in section 3.1, at a depth between about 60-70 m, variations in the Na, MSA and SO_4^{2-}/Na ratios no longer resolve annual cycles. Therefore, a gradual transition to incorporate more layers visible in the higher resolution calcium data was implemented. To confirm this transition, the time frame between 1285 CE and 1815 CE was also counted forward in time to assess the uncertainty in the chronology when transiting from high resolution to low resolution data. It should be noted that in the layer counting procedure, the depths
295   of the 1965 CE, 1285 CE, 1257 CE and 1229 CE tie points were considered to be fixed within one year, whereas the depth of the 1458 CE eruption was not. This difference is mainly due to the fact that around the 1458 CE depth the peak identification method switched from the sodium to calcium-dominated approach, leading to a larger age uncertainty in that depth interval. Only the calcium and conductivity records were used for annual layer counting below the depth of the 1229 CE eruption to 2,000 years before present. At this depth, annual layers were no longer resolved.
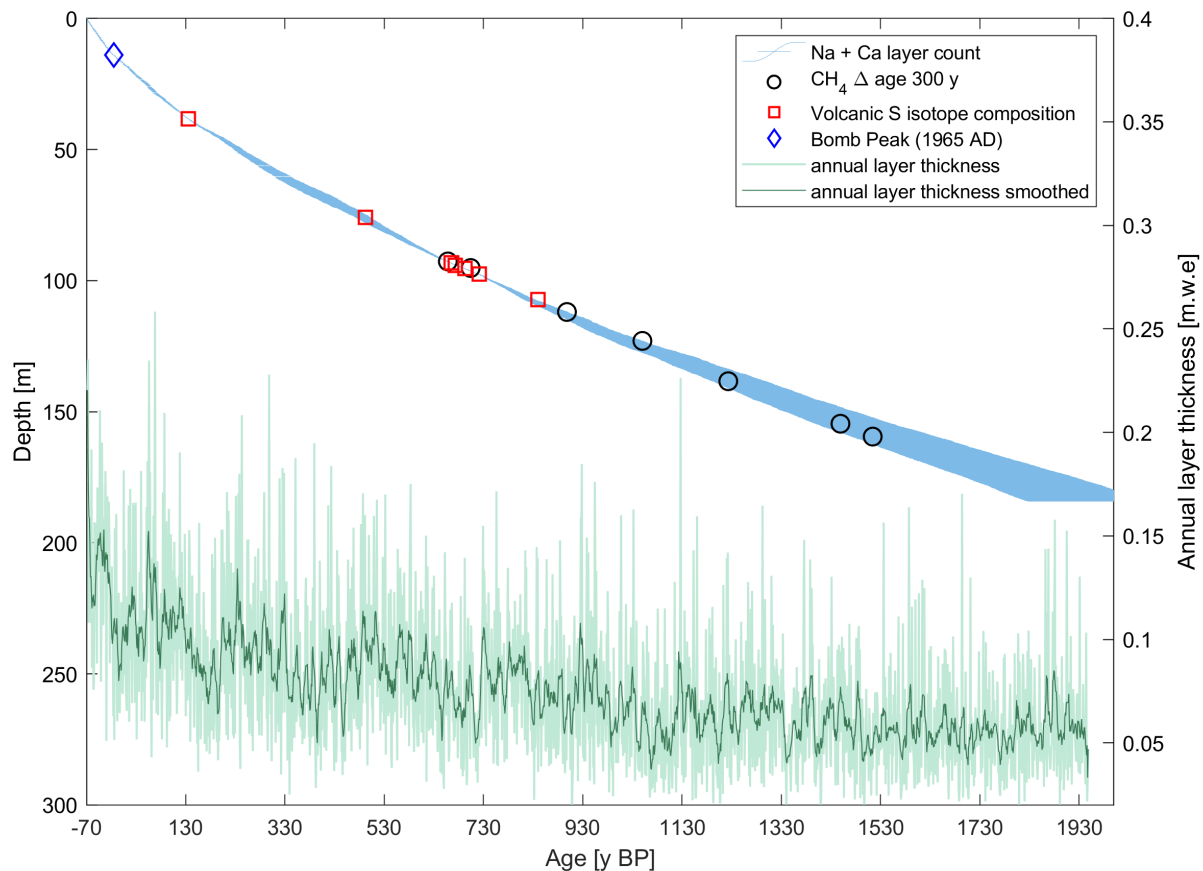
Figure 8. Stratigraphical depth-age relationship of the Skytrain ice core. The blue shaded area shows the annual layer counted chronology including the age uncertainty. The blue diamond marks the position of the tritium peak. The squares show the depth of identified volcanic eruptions and the circles show the methane reference points, assuming a delta age of 330 years. Note that the deepest volcanic eruption date should be considered only as potentially representing the 1110 CE (840 BP) eruption. The dark green line depicts the 10-year averaged evolution of the annual layer thickness with time, the light green is unsmoothed layer thickness.
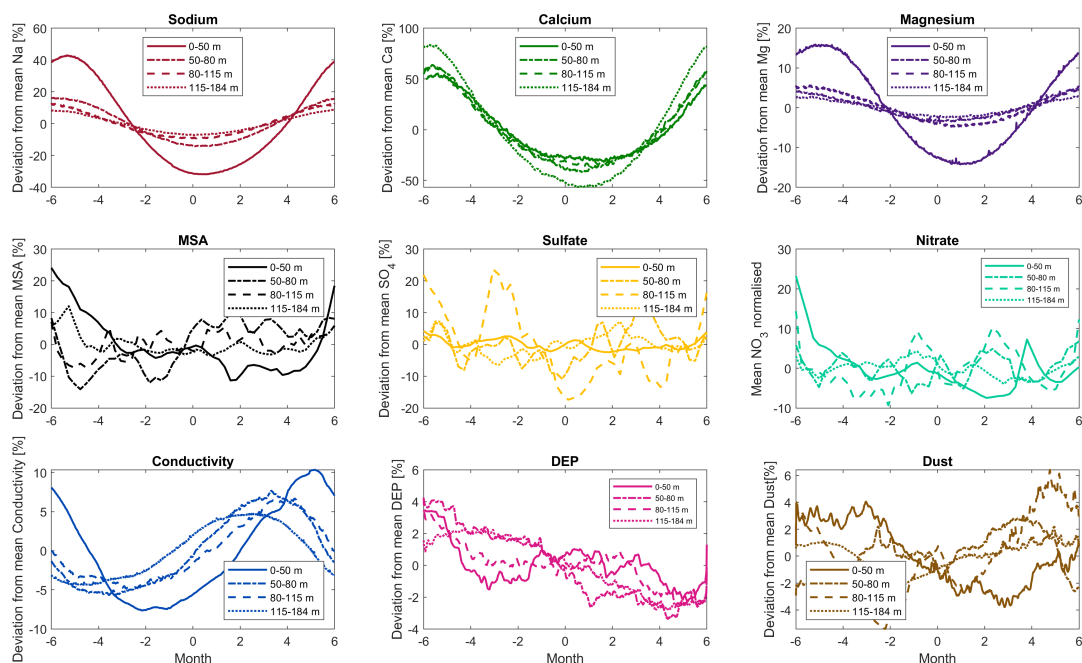
Figure 9. Seasonality analysis of main chemical species from CFA measurements. The horizontal axes show numbered months of the year, with zero denoting the first of January. The vertical axes show the normalised amplitude and the relative deviation from the annual mean of the respective signal for different depth intervals of the Skytrain ice core.

3.2.1 Investigation of seasonality

To better assess and quantify the seasonality in the signals of the most important chemical and physical markers (Na, Ca, Mg, MSA, SO_4^{2-} and conductivity), a more detailed investigation of the annual variations has been carried out similar to the procedure used by Winski et al. (2019). First, the CFA records within the annual intervals defined by the counting markers were interpolated over a twelve month period. Then, the CFA signals for the respective species were averaged for each month over different depth intervals of the core (0-50 m, 50-80 m, 80-115 m and 115-184 m). To normalise these mean concentrations and make them comparable, the monthly-averaged signals were subsequently divided by their respective annual mean. The relative deviations from the annual mean in percent are presented in Figure 9. The horizontal axes show the annual patterns of the signal over twelve months, with zero denoting the first of January. The depth intervals for averaging were chosen based on observations from the layer counting. The first one (0-50 m) mainly relied on the counting of the sodium and MSA peaks, the second on sodium and calcium and the last two mainly on calcium and conductivity.

The sodium signal shows the most distinct seasonality in the top 50 m, with maximum values in the Antarctic winter and deviations of more than 40% from the annual mean. In the deeper sections, the annual cyclicity is much less pronounced.

This is due to the fact that sodium was no longer the primary component for layer counting and also to the loss of resolution. Magnesium shows a very similar annual pattern, as expected (Curran et al., 1998), but with a maximum variation of about

315 15% from the annual mean much less distinct compared to the sodium. Calcium shows the highest amplitude seasonal cycle, with values up to 80% above the mean in the Antarctic winter. Calcium shows the strongest variation in the lowest investigated core section (115-184 m), which is caused by the fact that it was the main component for annual layer counting in this depth interval. However, the seasonality is also very pronounced in shallower depths, which supports the assumption that the total calcium signal is actually showing annual variations. MSA appears to have a seasonal variation in the top 50 m, where it was

320 also included in the counting scheme. For the deeper parts, the signal varies around the mean and no longer shows a cyclic trend. This result is mainly due to the very limited depth resolution of the FIC instrument. The low FIC resolution also affects the sulfate signal. Similar to the MSA signal, the sulfate also varies randomly around the mean and no obvious seasonality can be detected. This is also the case for the nitrate signal, which is influenced by the same limitation of depth resolution. The liquid conductivity signal appears to show a seasonal variation with a peak in Antarctic autumn. However, for conductivity the

325 deviation from the mean is only about 5%, which is very small compared to the other signal variations. There is a small drift in seasonality visible, which is most obvious between the top 50 m and the other depth intervals. This drift is very likely caused by the change in layer counting strategy around 60-70 m depth. The DEP signal should be expected to show a similar seasonality as the liquid conductivity, but unfortunately these measurements were also done with rather limited depth resolution. Therefore with this methodological approach, no seasonality in the DEP signal could be detected. The dust signal also does not show a

330 seasonality, which in this case it not caused by limited depth resolution, but (unlike some Greenland records for example) by a very noisy data set.

3.3 Chronology characteristics and the dating uncertainty

The combined approach of annual layer counting and the identification of absolute age markers led to a stratigraphical core chronology for the Skytrain ice core reaching back to 1942 $\pm$ 122 years before 1950 CE at 184.14 m total depth. The average

335 annual layer thickness varies between 0.1-0.15 m w.e. in the topmost part of the core to 0.05-0.1 m w.e. below about 90 m depth. There are two phases of accelerated layer thinning that are not related to changes in density (see Fig. 8). The first section is between $\sim$ 8-15 m total depth (-40 to -5 yBP), and the second is between $\sim$ 35-46 m total depth (120 - 200 yBP). We attribute these intervals of thinning, especially the second one, and the overall thinning in the top 90 m, to the effects of a distinctive Raymond Arch at the drilling site (Raymond, 1983), which has been detected by ground penetrating radar (Mulvaney et al.,

340 2021). The thinning and more rapid ageing effects of the ice due to this glaciological feature were underestimated in initial age-depth models and only became obvious after identification of the absolute age markers. We cannot rule out that changes in accumulation rate also contribute to the thinner layers.

The overall uncertainty of the ice core chronology consists of (i) the uncertainty in identification and counting of annual layers by the operator, (ii) the uncertainty of the depth and age assignment of the tie points and (iii) irregularities in the

345 stratigraphical order (e.g. missing layers). Therefore, a purely mathematical assessment of the error of the derived age-depth relationship is very difficult and all attempts at quantifying the dating uncertainty must be considered as estimates. By far the

largest source of error is missing or over-counting of annual layers by the operator, in combination with the limited resolution of the analytical methods. We tried to minimise these errors by using several independently measured chemical species simultaneously for annual layer counting as described above. (see Fig. 6). Based on the findings in section 3.2, we estimated three different counting error ranges for the core sections from 0-38.22 m (the depth of the Tambora eruption), 38.22-93.22 m (the depth of the 1285 CE eruption) and 97.45-184.11 m. These error ranges are shown as the blue shaded area in Fig. 8. For the topmost depth interval a cumulative age error of $\pm$ 5% was derived from two iterations of annual layer counting. This error increases with distance from the age markers (here the Tritium peak and the Tambora eruption) and was set to $\pm$ 1 year at the depths of the tie points. In the second depth interval the transition from the sodium to calcium dominated layer counting was performed. Together with a phase of layer thinning in this section, it was not possible to reduce the counting error to less than $\pm$ 8% at the depth of the presumed 1458 CE eruption (75.8m). Therefore, this volcanic marker was not used as a fixed tie point and the error range for the whole second depth interval was set to $\pm$ 8%. The depth range between the 1285 CE and 1229 CE tie points (93.25m-97.45m) was considered to have an age error of $\pm$ 1 years because this interval was used to calibrate and tune the counting procedure in the first place. In the deepest section, the error was estimated from the comparison of the counted chronology with the age markers derived from the methane measurements (black circles in Fig. 8). The cumulative error aimed to incorporate all of these age markers in its range, but they were not used as fixed tie points in the chronology. This approach led to an uncertainty range of $\pm$ 10% of the respective age in the section between 97.43 and 184.11 m. The highest uncertainty in the lowest section is also justified by the fact that the counting error will increase with depth due to the calcium fluorescence instrument resolution reaching its limitations at layer thicknesses below 5cm w.e. and the cumulative unconstrained counting error.

4   Conclusions

The first part of the ST22 chronology for Skytrain ice core covering the last 2000 years before present was successfully established. This time period of the most recent past is crucial for understanding current climate change processes and a well constrained chronology is a prerequisite for any further data interpretation. An age of 1950 BP was reached at a depth of 184.14 m. The dating of the ice core is based on stratigraphical methods. Annual layer counting has been carried out using primarily the sodium signal as a seasonal indicator in the top $\sim$ 60-70 m (about 300 years BP) and calcium for the lower part ($\sim$ 60 m - 184 m). The seasonality of the chosen parameters was also supported by power spectra analyses. The annual layer counting was finally constrained to a set of absolute age markers. These age markers include the tritium peak (1965 CE) and six volcanic eruptions identified via sulfur isotope analysis. Methane measurements were used to further verify the counted chronology, although they were not used as fixed age tie points. Based on the depth of the 1965 CE tritium peak, a surface accumulation of 13.5 cm w. e. / year was determined. The overall uncertainty of the record is dominated by counting errors of the operator. A minimum error of $\pm$ 1 year at the depths of the tie points was assumed. In between the tie points a cumulative age error of $\pm$ 5 % in the top part (0-38.22 m), $\pm$ 8 % in the middle part (38.22-93.22 m) and $\pm$ 10 % in the unconstrained bottom part (93.22-184 m) were determined. In the lowest part of the investigated core section, a gradual transition to the age model used

380 for the deep ice will be established (Mulvaney et al., 2022). The retrieved depth-age relationship was found to age much faster than expected from initial purely glaciological modeling. At least two phases of enhanced layer thinning at shallow core depths (above 90 m) were observed. This thinning is attributed to the influence of a pronounced Raymond Arch. The conservative uncertainty approach allows for interpretations on at least decadal time scales. Overall, the first part of the ST22 chronology provides a robust age-scale to interpret climatic signals recorded in the Skytrain ice core during the last 2000 years, as well as

385 for developing the age model for the deeper ice.

Data availability. The Skytrain Ice core Chronology data and some additional data regarding the sulfur isotope analysis can be found in the supplement.

Appendix A: Tritium samples data

Table A1. Sample data and results of the tritium measurements in the Skytrain ice core. The deepest 5 samples were below detection limit.

Depth absolute [m]	Depth [m.w.e.]	Mass water [g]	TU	Error TU
10.4	5.12	327	2.35	0.75
10.85	5.373	341	2.77	0.80
11.3	5.627	395	2.61	0.78
11.75	5.886	407	2.61	0.81
12.202	6.150	399	6.72	1.61
12.643	6.409	407	10.08	2.32
13.093	6.641	396	9.24	2.13
13.544	6.938	390	10.92	2.51
13.995	7.197	412	10.92	2.51
14.447	7.457	427	4.54	1.23
14.899	7.730	428	2.52	0.88
15.349	8.000	433	2.61	0.83
15.798	8.270	436	0.73	0.63
16.249	8.540	426	0.82	0.62
16.7	8.810	438	0.76	0.66
17.15	9.089	426	< 0.7	
17.6	9.370	438	< 0.7	
18.052	9.649	443	< 0.7	
18.502	9.925	444	< 0.7	
18.954	10.207	439	< 0.7	

Appendix B: Volcanic eruptions sulfur isotope data

Table B1. Sample data and results of the δ^{34}S and discrete sulfate measurements in the Skytrain ice core. Values are reported in permille, relative to VCDT. Data of the other samples that were not clearly identified can be found in the supplementary material.

Volcano [yCE]	Depth top [m]	Depth bottom [m]	δ^{34}S [‰]	Δ^{33}S [‰]	SO_4 [ppb]
1815	38.22	38.29	10.94	0.28	149.81
1458	75.75	75.8	3.76	-0.03	405.52
1458	75.8	75.85	4.89	0.19	369.05
1285	93.22	93.27	4.47	-0.40	145.96
1276	94.08	94.15	13.37	-0.03	66.57
1257	95.18	95.23	-4.84	-1.26	168.07
1257	95.23	95.28	-12.31	-1.36	138.15
1257	95.28	95.33	9.21	0.39	430.34
1257	95.33	95.38	17.19	0.93	275.30
1229	97.43	97.48	4.07	-0.45	115.48
1110?	107.26	107.31	14.32	- 0.24	203.58

Appendix C: Methane age tie points

Table C1. Age reference points picked from visual comparison of Skytrain, WAIS divide and Antarctic composite methane data. A delta age of 300 years was used to convert gas age into ice age for Skytrain ice core.

Depth [m]	CH_4 [ppb]	Gas age [yBP]	Ice age [yBP]
92.7	683.6	357	657
95.2	717.7	395	695
111.98	679.4	595	895
123	695	752	1052
138.39	686.3	923	1223
154.6	627.4	1149	1449
159.5	656.8	1214	1514

Author contributions. The paper was written by HH with contributions from AK, MG, HP, DV, CN-A, EW and AS. The ice core was drilled and processed by EW, RM, CN-A, MG, IR, ED and AK. The CFA analysis was performed by HH, MG, JH, RM, ET and IR. The tritium

measurements were done by AS. The sulfur isotope analysis was done by ED and HP. The methane measurements were produced by AK, JE, KM and DV. The annual layer counting and development of the core chronology together with the uncertainty estimation and seasonality

395   investigations were produced by HH and EW. All authors contributed to improving the final paper.

Competing interests. The authors declare that they have no competing interests.

Acknowledgements. The authors thank Shaun Miller, Emily Ludlow, and Victoria Alcock for help with cutting and processing the ice core. The authors also thank Charlie Durman for ice core preparation for the CFA analysis. This project has received funding from the European Research Council under the Horizon 2020 research and innovation programme (grant agreement No 742224, WACSWAIN). This material

400   reflects only the author's views and the Commission is not liable for any use that may be made of the information contained therein. EW and HH have also been funded for part of this work through a Royal Society Professorship.

References

Baroni, M., Savarino, J., Cole-Dai, J., Rai, V. K., and Thiemens, M. H.: Anomalous sulfur isotope compositions of vol-
canic sulfate over the last millennium in Antarctic ice cores, Journal of Geophysical Research: Atmospheres, 113,
https://doi.org/https://doi.org/10.1029/2008JD010185, 2008.

Bigler, M., Svensson, A., Kettner, E., Vallelonga, P., Nielsen, M. E., and Steffensen, J. P.: Optimization of High-Resolution
Continuous Flow Analysis for Transient Climate Signals in Ice Cores, Environmental Science & Technology, 45, 4483–4489,
https://doi.org/10.1021/es200118j, pMID: 21504155, 2011.

Bromwich, D. H., Nicolas, J. P., Monaghan, A. J., Lazzara, M. A., Keller, L. M., Weidner, G. A., and Wilson, A. B.: Central West Antarctica
among the most rapidly warming regions on Earth, Nature Geoscience, 6, 139–145, https://doi.org/10.1038/ngeo1671, 2013.

Burke, A., Moore, K. A., Sigl, M., Nita, D. C., McConnell, J. R., and Adkins, J. F.: Stratospheric eruptions from tropical and extra-tropical
volcanoes constrained using high-resolution sulfur isotopes in ice cores, Earth and planetary science letters, 521, 113–119, 2019.

Castellano, E., Becagli, S., Hansson, M., Hutterli, M., Petit, J., Rampino, M., Severi, M., Steffensen, J. P., Traversi, R., and Udisti, R.:
Holocene volcanic history as recorded in the sulfate stratigraphy of the European Project for Ice Coring in Antarctica Dome C (EDC96)
ice core, Journal of Geophysical Research: Atmospheres, 110, https://doi.org/10.1029/2004JD005259, 2005.

Craddock, P. R., Rouxel, O. J., Ball, L. A., and Bach, W.: Sulfur isotope measurement of sulfate and sulfide by high-resolution MC-ICP-MS,
Chemical Geology, 253, 102–113, 2008.

Curran, M. A., Van Ommen, T. D., and Morgan, V.: Seasonal characteristics of the major ions in the high-accumulation Dome Summit South
ice core, Law Dome, Antarctica, Annals of Glaciology, 27, 385–390, https://doi.org/10.3189/1998AoG27-1-385-390, 1998.

Dalaiden, Q., Goosse, H., Klein, F., Lenaerts, J. T. M., Holloway, M., Sime, L., and Thomas, E. R.: How useful is snow accumulation
in reconstructing surface air temperature in Antarctica? A study combining ice core records and climate models, The Cryosphere, 14,
1187–1207, https://doi.org/10.5194/tc-14-1187-2020, https://tc.copernicus.org/articles/14/1187/2020/, 2020.

Das, A., Chung, C.-H., You, C.-F., and Shen, M.-L.: Application of an improved ion exchange technique for the measurement of δ 34 S
values from microgram quantities of sulfur by MC-ICPMS, Journal of Analytical Atomic Spectrometry, 27, 2088–2093, 2012.

DeConto, R. M. and Pollard, D.: Contribution of Antarctica to past and future sea-level rise, Nature, 531, 591–597,
https://doi.org/10.1038/nature17145, 2016.

Dixon, D., Mayewski, P. A., Kaspari, S., Sneed, S., and Handley, M.: A 200 year sub-annual record of sulfate in West Antarctica, from 16
ice cores, Annals of Glaciology, 39, 545–556, https://doi.org/10.3189/172756404781814113, 2004.

Dlugokencky, E. J., Myers, R. C., Lang, P. M., Masarie, K. A., Crotwell, A. M., Thoning, K. W., Hall, B. D., Elkins, J. W., and Steele,
L. P.: Conversion of NOAA atmospheric dry air CH4 mole fractions to a gravimetrically prepared standard scale, Journal of Geophysical
Research: Atmospheres, 110, https://doi.org/https://doi.org/10.1029/2005JD006035, 2005.

Dunbar, N. W., Zielinski, G. A., and Voisins, D. T.: Tephra layers in the Siple Dome and Taylor Dome ice cores, Antarctica: Sources and
correlations, Journal of Geophysical Research: Solid Earth, 108, https://doi.org/https://doi.org/10.1029/2002JB002056, 2003.

Emanuelsson, B. D., Thomas, E. R., Tetzner, D. R., Humby, J. D., and Vladimirova, D. O.: Ice Core Chronologies from the Antarctic
Peninsula: The Palmer, Jurassic, and Rendezvous Age-Scales, Geosciences, 12, https://doi.org/10.3390/geosciences12020087, 2022.

Epifanio, J. A., Brook, E. J., Buizert, C., Edwards, J. S., Sowers, T. A., Kahle, E. C., Severinghaus, J. P., Steig, E. J., Winski, D. A.,
Osterberg, E. C., Fudge, T. J., Aydin, M., Hood, E., Kalk, M., Kreutz, K. J., Ferris, D. G., and Kennedy, J. A.: The SP19 chronology

for the South Pole Ice Core – Part 2: gas chronology, Δage, and smoothing of atmospheric records, Climate of the Past, 16, 2431–2444, https://doi.org/10.5194/cp-16-2431-2020, https://cp.copernicus.org/articles/16/2431/2020/, 2020.

440   Farquhar, J., Savarino, J., Airieau, S., and Thiemens, M. H.: Observation of wavelength-sensitive mass-independent sulfur isotope effects during SO2 photolysis: Implications for the early atmosphere, Journal of Geophysical Research: Planets, 106, 32 829–32 839, 2001.

Fourré, E., Jean-Baptiste, P., Dapoigny, A., Baumier, D., Petit, J.-R., and Jouzel, J.: Past and recent tritium levels in Arctic and Antarctic polar caps, Earth and Planetary Science Letters, 245, 56–64, https://doi.org/https://doi.org/10.1016/j.epsl.2006.03.003, https://www.sciencedirect.com/science/article/pii/S0012821X06002081, 2006.

445   Fourré, E., Landais, A., Cauquoin, A., Jean-Baptiste, P., Lipenkov, V., and Petit, J.-R.: Tritium Records to Trace Stratospheric Moisture Inputs in Antarctica, Journal of Geophysical Research: Atmospheres, 123, 3009–3018, https://doi.org/https://doi.org/10.1002/2018JD028304, 2018.

Gautier, E., Savarino, J., Hoek, J., Erbland, J., Caillon, N., Hattori, S., Yoshida, N., Albalat, E., Albarede, F., and Farquhar, J.: 2600-years of stratospheric volcanism through sulfate isotopes, Nature communications, 10, 1–7, 2019.

450   Grachev, A. M., Brook, E. J., Severinghaus, J. P., and Pisias, N. G.: Relative timing and variability of atmospheric methane and GISP2 oxygen isotopes between 68 and 86 ka, Global Biogeochemical Cycles, 23, https://doi.org/https://doi.org/10.1029/2008GB003330, https://agupubs.onlinelibrary.wiley.com/doi/abs/10.1029/2008GB003330, 2009.

Grieman, M. M., Hoffmann, H. M., Humby, J. D., Mulvaney, R., Nehrbass-Ahles, C., Rix, J., Thomas, E. R., Tuckwell, R., and Wolff, E. W.: Continuous flow analysis methods for sodium, magnesium and calcium detection in the Skytrain ice core, Journal of Glaciology, p. 1–11,
455   https://doi.org/10.1017/jog.2021.75, 2021.

Koehler, P., Nehrbass-Ahles, C., Schmitt, J., Stocker, T. F., and Fischer, H.: A 156 kyr smoothed history of the atmospheric greenhouse gases CO_2, CH_4, and N_2O and their radiative forcing, Earth System Science Data, 9, 363–387, https://doi.org/10.5194/essd-9-363-2017, https://essd.copernicus.org/articles/9/363/2017/, 2017.

Lee, J. E., Brook, E. J., Bertler, N. A. N., Buizert, C., Baisden, T., Blunier, T., Ciobanu, V. G., Conway, H., Dahl-Jensen, D., Fudge, T. J.,
460   Hindmarsh, R., Keller, E. D., Parrenin, F., Severinghaus, J. P., Vallelonga, P., Waddington, E. D., and Winstrup, M.: An 83 000-year-old ice core from Roosevelt Island, Ross Sea, Antarctica, Climate of the Past, 16, 1691–1713, https://doi.org/10.5194/cp-16-1691-2020, https://cp.copernicus.org/articles/16/1691/2020/, 2020.

Loulergue, L., Parrenin, F., Blunier, T., Barnola, J.-M., Spahni, R., Schilt, A., Raisbeck, G., and Chappellaz, J.: New constraints on the gas age-ice age difference along the EPICA ice cores, 0-50 kyr, Climate of the Past, 3, 527–540, https://doi.org/10.5194/cp-3-527-2007,
465   https://cp.copernicus.org/articles/3/527/2007/, 2007.

MacFarling Meure, C., Etheridge, D., Trudinger, C., Steele, P., Langenfelds, R., van Ommen, T., Smith, A., and Elkins, J.: Law Dome CO2, CH4 and N2O ice core records extended to 2000 years BP, Geophysical Research Letters, 33, https://doi.org/https://doi.org/10.1029/2006GL026152, https://agupubs.onlinelibrary.wiley.com/doi/abs/10.1029/2006GL026152, 2006.

Mekhaldi, F., Muscheler, R., Adolphi, F., Aldahan, A., Beer, J. McConnell, J. R., Possnert, G., Sigl, M., Svensson, A., Synal, H.-A., Welten,
470   K. C., and Woodruff, T. E.: Multiradionuclide evidence for the solar origin of the cosmic-ray events of AD 774/5 and 993/4, Nature Communications, 6, https://doi.org/10.1038/ncomms9611, 2015.

Mitchell, L., Brook, E., Lee, J. E., Buizert, C., and Sowers, T.: Constraints on the Late Holocene Anthropogenic Contribution to the Atmospheric Methane Budget, Science, 342, 964–966, https://doi.org/10.1126/science.1238920, https://www.science.org/doi/abs/10.1126/science.1238920, 2013.

475   Mitchell, L. E., Brook, E. J., Sowers, T., McConnell, J. R., and Taylor, K.: Multidecadal variability of atmospheric methane, 1000–1800 C.E., Journal of Geophysical Research: Biogeosciences, 116, https://doi.org/https://doi.org/10.1029/2010JG001441, https://agupubs. onlinelibrary.wiley.com/doi/abs/10.1029/2010JG001441, 2011.

Morishima, H., Kawai, H., Koga, T., and Niwa, T.: The Trends of Global Tritium Precipitations, Journal of Radiation Research, 26, 283–312, https://doi.org/10.1269/jrr.26.283, https://doi.org/10.1269/jrr.26.283, 1985.

480   Mulvaney, R., Rix, J., Polfrey, S., Grieman, M., Martìn, C., Nehrbass-Ahles, C., Rowell, I., Tuckwell, R., and Wolff, E.: Ice drilling on Skytrain Ice Rise and Sherman Island, Antarctica, Annals of Glaciology, p. 1–13, https://doi.org/10.1017/aog.2021.7, 2021.

Mulvaney, R., Wolff, E., Grieman, M., Hoffmann, H., Humby, J., Rowell, I., Parrenin, F., Rhodes, R., Martin, C., Kingslake, J., Nehrbass-Ahles, C., Schmidely, L., Fischer, H., Stocker, T., Christl, M., Muscheler, R., Landais, A., and Prié, F.: The ST21 chronology for the Skytrain Ice Rise ice core - part 2: an age model to the last interglacial and disturbed deep stratigraphy, Climate of the Past, p. in prep.,
485   2022.

Nielsen, H., Pilot, J., Grinenko, L., Grinenko, V., Lein, A. Y., Smith, J., and Pankina, R.: Lithospheric sources of sulphur, in: Stable isotopes: natural and anthropogenic sulphur in the environment, 1991.

Osman, M., Das, S. B., Marchal, O., and Evans, M. J.: Methanesulfonic acid (MSA) migration in polar ice: data synthesis and theory., Cryosphere, 11, https://doi.org/10.5194/tc-11-2439-2017, 2017.

490   Paris, G., Sessions, A. L., Subhas, A. V., and Adkins, J. F.: MC-ICP-MS measurement of $\delta34S$ and $\Delta 33S$ in small amounts of dissolved sulfate, Chemical Geology, 345, 50–61, 2013.

Parrenin, F., Rémy, F., Ritz, C., Siegert, M. J., and Jouzel, J.: New modeling of the Vostok ice flow line and implication for the glaciological chronology of the Vostok ice core, Journal of Geophysical Research: Atmospheres, 109, https://doi.org/https://doi.org/10.1029/2004JD004561, 2004.

495   Pasteur, E. C. and Mulvaney, R.: Migration of methane sulphonate in Antarctic firn and ice, Journal of Geophysical Research: Atmospheres, 105, 11 525–11 534, https://doi.org/https://doi.org/10.1029/2000JD900006, https://agupubs.onlinelibrary.wiley.com/doi/abs/10. 1029/2000JD900006, 2000.

Patris, N., Delmas, R. J., and Jouzel, J.: Isotopic signatures of sulfur in shallow Antarctic ice cores, Journal of Geophysical Research: Atmospheres, 105, 7071–7078, 2000.

500   Philippe, M., Tison, J.-L., Fjøsne, K., Hubbard, B., Kjær, H. A., Lenaerts, J. T. M., Drews, R., Sheldon, S. G., De Bondt, K., Claeys, P., and Pattyn, F.: Ice core evidence for a 20th century increase in surface mass balance in coastal Dronning Maud Land, East Antarctica, The Cryosphere, 10, 2501–2516, https://doi.org/10.5194/tc-10-2501-2016, https://tc.copernicus.org/articles/10/2501/2016/, 2016.

Preunkert, S., Jourdain, B., Legrand, M., Udisti, R., Becagli, S., and Cerri, O.: Seasonality of sulfur species (dimethyl sulfide, sulfate, and methanesulfonate) in Antarctica: Inland versus coastal regions, Journal of Geophysical Research: Atmospheres, 113,
505   https://doi.org/https://doi.org/10.1029/2008JD009937, https://agupubs.onlinelibrary.wiley.com/doi/abs/10.1029/2008JD009937, 2008.

Rasmussen, S. O., Andersen, K. K., Svensson, A. M., Steffensen, J. P., Vinther, B. M., Clausen, H. B., Siggaard-Andersen, M.-L., Johnsen, S. J., Larsen, L. B., Dahl-Jensen, D., Bigler, M., Röthlisberger, R., Fischer, H., Goto-Azuma, K., Hansson, M. E., and Ruth, U.: A new Greenland ice core chronology for the last glacial termination, Journal of Geophysical Research: Atmospheres, 111, https://doi.org/https://doi.org/10.1029/2005JD006079, 2006.

510   Rasmussen, S. O., Seierstad, I. K., Andersen, K. K., Bigler, M., Dahl-Jensen, D., and Johnsen, S. J.: Synchronization of the NGRIP, GRIP, and GISP2 ice cores across MIS 2 and palaeoclimatic implications, Quaternary Science Reviews, 27, 18–28, https://doi.org/10.1016/j.quascirev.2007.01.016, 2008.

Raymond, C. F.: Deformation in the Vicinity of Ice Divides, Journal of Glaciology, 29, 357–373, https://doi.org/10.3189/S0022143000030288, 1983.

515 Rees, C., Jenkins, W., and Monster, J.: The sulphur isotopic composition of ocean water sulphate, Geochimica et Cosmochimica Acta, 42, 377–381, https://doi.org/https://doi.org/10.1016/0016-7037(78)90268-5, https://www.sciencedirect.com/science/article/pii/0016703778902685, 1978.

Savarino, J., Romero, A., Cole-Dai, J., Bekki, S., and Thiemens, M.: UV induced mass-independent sulfur isotope fractionation in stratospheric volcanic sulfate, Geophysical Research Letters, 30, 2003.

520 Schlosser, E. and Oerter, H.: Seasonal variations of accumulation and the isotope record in ice cores: a study with surface snow samples and firn cores from Neumayer station, Antarctica, Annals of Glaciology, 35, 97–101, https://doi.org/10.3189/172756402781817374, 2002.

Schmidt, A., Frank, G., Stichler, W., Duester, L., Steinkopff, T., and Stumpp, C.: Overview of tritium records from precipitation and surface waters in Germany, Hydrological Processes, 34, 1489–1493, https://doi.org/https://doi.org/10.1002/hyp.13691, https://onlinelibrary.wiley.com/doi/abs/10.1002/hyp.13691, 2020.

525 Schüpbach, S., Fischer, H., Bigler, M., Erhardt, T., Gfeller, G., Leuenberger, D., Mini, O., Mulvaney, R., Abram, N., Fleet, L., Frey, M., Thomas, E., Svensson, A., Dahl-Jensen, D., Kettner, E., Kjaer, H., Seierstad, I., Steffensen, J., Rasmussen, S., Vallelonga, P., Winstrup, M., Wegner, A., Twarloh, B., Wolff, K., Schmidt, K., Goto-Azuma, K., Kuramoto, T., Hirabayashi, M., Uetake, J., Zheng, J., Bourgeois, J., Fisher, D., Zhiheng, D., Xiao, C., Legrand, M., Spolaor, A., Gabrieli, J., Barbante, C., Kang, J., Hur, S., Hong, S., Hwang, H., Hong, S., Hansson, M., Iizuka, Y., Oyabu, I., Muscheler, R., Adolphi, F., Maselli, O., McConnell, J., and Wolff, E.: Greenland records of aerosol

530 source and atmospheric lifetime changes from the Eemian to the Holocene, Nature Communications, 9, https://doi.org/10.1038/s41467-018-03924-3, 2018.

Sigg, A. and Neftel, A.: Seasonal variations in hydrogen peroxide in polar ice cores, Annals of Glaciology, 10, 157–162, https://doi.org/10.3189/S0260305500004353, 1988.

Sigl, M., Winstrup, M., McConnell, J. R., Welten, K. C., Plunkett, G., Ludlow, F., Büntgen, U., Caffee, M., Chellman, N.,

535 Dahl-Jensen, D., et al.: Timing and climate forcing of volcanic eruptions for the past 2,500 years, Nature, 523, 543–549, https://doi.org/10.1038/nature14565, 2015.

Sigl, M., Fudge, T. J., Winstrup, M., Cole-Dai, J., Ferris, D., McConnell, J. R., Taylor, K. C., Welten, K. C., Woodruff, T. E., Adolphi, F., et al.: The WAIS Divide deep ice core WD2014 chronology–Part 2: Annual-layer counting (0–31 ka BP), Climate of the Past, 12, 769–786, https://doi.org/10.5194/cp-12-769-2016, 2016.

540 Sigl, M., Buizert, C., Fudge, T. J., Winstrup, M., Cole-Dai, J., McConnell, J. R., Ferris, D. G., Rhodes, R. H., Taylor, K. C., Welten, K. C., Woodruff, T. E., Adolphi, F., Baggenstos, D., Brook, E. J., Caffee, M. W., Clow, G. D., Cheng, H., Cuffey, K. M., Dunbar, N. W., Edwards, R. L., Edwards, L., Geng, L., Iverson, N., Koffman, B. G., Layman, L., Markle, B. R., Maselli, O. J., McGwire, K. C., Muscheler, R., Nishiizumi, K., Pasteris, D. R., Severinghaus, J. P., Sowers, T. A., and Steig, E. J.: WAIS Divide Deep ice core 0-68 ka WD2014 chronology, https://doi.org/10.1594/PANGAEA.902577, https://doi.org/10.1594/PANGAEA.902577, 2019.

545 Taylor, C. B.: Tritium Content of Antarctic Snow, Nature, 201, https://doi.org/10.1038/201146a0, 1964.

Tetzner, D. R., Thomas, E. R., Allen, C. S., and Piermattei, A.: Evidence of Recent Active Volcanism in the Balleny Islands (Antarctica) From Ice Core Records, Journal of Geophysical Research: Atmospheres, 126, e2021JD035 095, https://doi.org/https://doi.org/10.1029/2021JD035095, https://agupubs.onlinelibrary.wiley.com/doi/abs/10.1029/2021JD035095, 2021.

USGS, NASA, B.: Landsat Image Mosaic Of Antarctica (LIMA), https://lima.usgs.gov/documents/LIMA_overview_map.pdf, 1999.

550   Wagenbach, D., Görlach, U., Moser, K., and Münnich, K. O.: Coastal Antarctic aerosol: the seasonal pattern of its chemical composition and radionuclide content, Tellus B: Chemical and Physical Meteorology, 40, 426–436, https://doi.org/10.3402/tellusb.v40i5.16010, 1988.

Wilhelms, F., Kipfstuhl, J., Miller, H., Heinloth, K., and Firestone, J.: Precise dielectric profiling of ice cores: a new device with improved guarding and its theory, Journal of Glaciology, 44, 171–174, https://doi.org/10.3189/S002214300000246X, 1998.

Winski, D. A., Fudge, T. J., Ferris, D. G., Osterberg, E. C., Fegyveresi, J. M., Cole-Dai, J., Thundercloud, Z., Cox, T. S., Kreutz, K. J.,
555   Ortman, N., et al.: The SP19 chronology for the South Pole Ice Core–Part 1: volcanic matching and annual layer counting, Climate of the Past, 15, https://doi.org/10.5194/cp-15-1793-2019, 2019.

Winstrup, M., Svensson, A. M., Rasmussen, S. O., Winther, O., Steig, E. J., and Axelrod, A. E.: An automated approach for annual layer counting in ice cores, Climate of the Past, 8, 1881–1895, https://doi.org/10.5194/cp-8-1881-2012, https://cp.copernicus.org/articles/8/1881/2012/, 2012.

560   Winstrup, M., Vallelonga, P., Kjær, H. A., Fudge, T. J., Lee, J. E., Riis, M. H., Edwards, R., Bertler, N. A., Blunier, T., Brook, E. J., et al.: A 2700-year annual timescale and accumulation history for an ice core from Roosevelt Island, West Antarctica, Climate of the Past, 15, 751–779, https://doi.org/10.5194/cp-15-751-2019, 2019.